A six-legged piano stool dysprosium single-molecule magnet

Sophie C. Corner,[a] *William J. A. Blackmore,*[a] *Gemma K. Gransbury,*[a] *George F. S. Whitehead,*[a] *Nicholas F. Chilton*[a,b]* *and David P. Mills*[a]*

[a]Department of Chemistry, The University of Manchester, Oxford Road, Manchester, M13 9PL, U.K.

[b]Research School of Chemistry, The Australian National University, Building 137, Sullivans Creek Road, Canberra, ACT, 2601, Australia

*Email: nicholas.chilton@anu.edu.au, david.mills@manchester.ac.uk.

Abstract

Dysprosium single-molecule magnets (SMMs) with two mutually *trans*- anionic ligands have shown large crystal field (CF) splitting, giving record effective energy barriers to magnetic reversal (U_{eff}) and hysteresis temperatures (T_H). However, these complexes tend to be bent, imposing a transverse field that reduces the purity of the m_J projections of the CF states and promotes magnetic relaxation. A complex with only one anionic ligand could have more pure CF states, and thus high U_{eff} and T_H. Here we report the first example of an SMM with this topology, $[Dy(C_5Me_5)(FPh)_6][\{Al[OC(CF_3)_3]_3\}_2(\mu\text{-}F)]_2$ (**1-Dy**), which exhibits U_{eff} = 564(33) cm^{-1} and T_H = 14 K at sweep rates of 22 Oe s^{-1}; the C_5Me_5 ligand imposes a strong axial CF and the five equatorially-bound neutral fluorobenzenes present only weak transverse interactions. We show that complexes such as **1-Dy** can be useful starting materials for heteroleptic Ln complexes as the fluorobenzenes are easily displaced.

Introduction

Single-molecule magnets (SMMs) show magnetic remanence,[1] and lanthanide (Ln) SMMs have provided the largest effective energy barriers to magnetic reversal (U_{eff}) and hysteresis temperatures (T_H) to date.[2–4] These advances have been driven by classical electrostatic design criteria to increase magnetic anisotropy, where Dy(III) and Tb(III) SMMs with two mutually *trans*-anionic ligands show the largest U_{eff} from stabilising the largest $\pm m_J$ projections in the ground state and destabilising the smaller $\pm m_J$ states.[5–7] Perfectly linear (i.e. with a C_∞ axis) Dy(III) and Tb(III) complexes would have pure $\pm m_J$ states, which would suppress two-phonon Raman and quantum tunnelling of magnetization (QTM) relaxation processes, giving high T_H values. However, any deviation from linearity introduces transverse fields that mix the m_J states, reducing T_H. Given the difficulty of isolating linear Ln(III) complexes, we considered that a Dy(III) complex with only a single anionic ligand may show purer $\pm m_J$ states than a bent *bis*-anionic complex and hence show relatively high T_H. Indeed, the theoretical $[DyO]^+$ cation has been predicted to have $U_{eff} > 2084$ cm^{-1},[6] but the isolation of such a coordinatively unsaturated complex is inherently challenging due to a combination of large Ln cations and predominantly ionic bonding regimes favouring high coordination numbers.[8] The closest molecular analogues of $[DyO]^+$ are endohedral fullerenes containing $\{Dy_2O\}$ fragments,[9–12] and these compounds show favourable SMM properties, but magnetic relaxation is promoted by interactions of Dy(III) ions with the anionic cages.

The first Dy(III) complex containing no equatorially-bound ligands, $[Dy(Cp^{ttt})_2][B(C_6F_5)_4]$ ($Cp^{ttt} = C_5H_2{}^tBu_3$-1,2,4), was reported in 2017; this SMM showed $U_{eff} = 1223(15)$ cm^{-1} and $T_H =$ 60 K due to a combination of the axial ligand field and rigid aromatic Cp^R (substituted cyclopentadienyl) rings hindering both Orbach and Raman relaxation.[13] Related Ln SMMs with higher U_{eff} and T_H values have since been achieved by decreasing Ln–L (L = ligand) distances and

increasing L–Ln–L angles,[14–16,17–20,21] and in an extension of this methodology the dinuclear complex [{Dy($C_5^iPr_5$)}$_2$(μ-I)$_3$] shows T_H = 80 K and U_{eff} = 1631(25) cm^{-1}.[22] Although smaller Cp^R ligands allow shorter Ln–L distances (and thus could improve U_{eff}), they also permit less bulky [Dy(Cp^R)$_2$]$^+$ cations to have more bent geometries, which leads to lower purity $\pm m_J$ states, faster Raman relaxation, and lower T_H.[23,24] Indeed, one of the smallest possible Cp^R ligands Cp* = C_5Me_5 tends to form bent Dy(III) *bis*-Cp* complexes with equatorially-bound ligands, which have all showed low T_H (< 12 K).[25,26] Recently, we have been exploring the effect of weak equatorial binding of neutral halobenzenes to bent [Dy(Cp^R)$_2$]$^+$ cations,[26,27] finding that they provide only minor disruption to the axiality if the complex geometry is preserved. We hypothesised that a fluorobenzene adduct of a *mono*-Cp* Dy(III) dication [Dy(Cp*)(FPh)$_n$]$^{2+}$ would show reduced U_{eff} due to having only one Cp^R ligand, but should have increased purity of low-lying $\pm m_J$ states *vs.* bent *bis*-Cp* cations and thus achieve a relatively high T_H. Aside from magnetic properties, rare earth alkyl dications can be effective olefin polymerisation catalysts,[28] but to the best of our knowledge the only previous structurally authenticated Ln(III) mono-cyclopentadienyl dication[29] was seen in [Tm(Cp*)(NCMe)$_6$][I]$_2$ (Cp* = C_5Me_5).[30]

Here we report the six-legged piano stool Ln(III) complexes [Ln(Cp*)(FPh)$_6$][{Al[OC(CF$_3$)$_3$]$_3$}$_2$(μ-F)]$_2$ (**1-Ln**; Ln = Y, Dy) and their characterisation by elemental analysis, NMR and ATR-IR spectroscopy, powder and single crystal XRD, SQUID magnetometry, and density functional theory (DFT) and complete active space self-consistent field spin-orbit (CASSCF-SO) calculations. Despite the modest U_{eff} = 564(33) cm^{-1} for **1-Dy**, its T_H = 14 K is similar to the best-performing Dy(III) *bis*-Cp* complexes reported to date.[25,26] Finally, the salt metathesis reactions of **1-Y** with s-block ligand transfer agents are shown to proceed cleanly at

room temperature, thus **1-Ln** are also useful starting materials to heteroleptic Ln complexes as weakly-bound fluorobenzenes are easily displaced.[31]

Results

Synthesis. The solvent-free Ln(III) Cp* borohydride precursors $[Ln(Cp^*)(\mu\text{-}BH_4)_2]_\infty$ (**2-Ln**; Ln = Y, Dy) were synthesised in 64–73% yields by the respective stoichiometric salt metathesis reactions of parent $[Ln(BH_4)_3(THF)_3]$[32] with KCp^*[33] in THF, followed by desolvation under reduced pressure (150 °C, 10^{-3} mbar) and recrystallisation from benzene or toluene. The abstraction of two hydrides from **2-Ln** with concomitant installation of two weakly coordinating anions (WCAs) and elimination of diborane using two equivalents of $[CPh_3][\{Al[OC(CF_3)_3]_3\}_2(\mu\text{-}F)]$[34] in fluorobenzene at 70 °C proceeded to completion in 30 min; the target complexes **1-Ln** were isolated in 58–64% yields following work-up and recrystallisation from fluorobenzene solutions layered with hexane (Fig. 1). Initial attempts to synthesise $[Dy(Cp^*)(FPh)_6][Al\{OC(CF_3)_3\}_4]_2$ from **2-Dy** and $[CPh_3][Al\{OC(CF_3)_3\}_4]$[35] under analogous conditions gave several crystals of a Dy(III) *bis*-alkoxide byproduct, $[Dy\{OC(CF_3)_3\}_2(FPh)_5][\{Al[OC(CF_3)_3]_3\}_2(\mu\text{-}F)]$ (**3-Dy**); the mechanism of formation of **3-Dy** is unknown but likely proceeds *via* the abstraction of $\{OC(CF_3)_3\}$ from $[Al\{OC(CF_3)_3\}_4]^-$ to generate the WCA, promoted by the Lewis acidic Dy(III) centre. As only a trace amount of **3-Dy** was isolated its characterisation was limited to single crystal XRD.

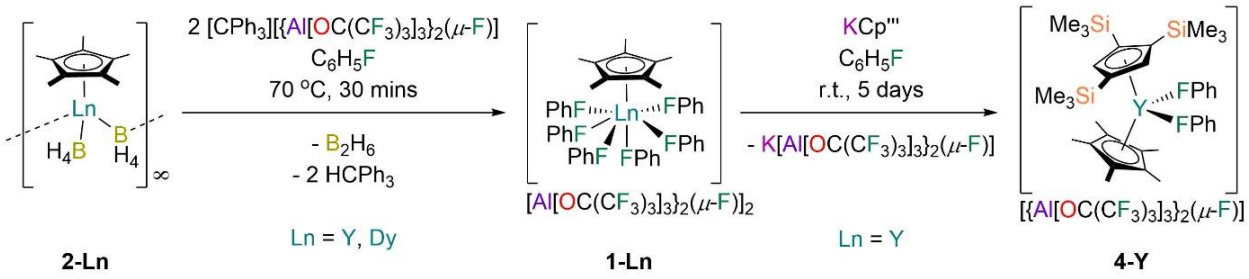

Fig. 1. Synthesis of **1-Ln** (Ln = Y, Dy) by the separate reactions of parent **2-Ln** with $[CPh_3][\{Al[OC(CF_3)_3]_3\}_2(\mu\text{-F})]$ in fluorobenzene and synthesis of **4-Y** by the reaction of **1-Y** with KCp‴ in fluorobenzene.

We envisaged that **1-Ln** could be useful precursors to novel heteroleptic Ln complexes as the coordinated fluorobenzenes will be easily displaced in salt metathesis reactions,[31] allowing a second bulky anionic ligand to be installed without the need for forcing conditions that can lead to byproduct formation. e.g. by cyclometallation.[36] We have previously shown that Ln complexes coordinated by Cp‴ ($\{C_5H_2(SiMe_3)_3\text{-}1,3\}$) are prone to decomposition reactions with anion abstraction reagents due to facile cleavage of the weak C–Si bonds, thus isolated Ln metallocenium cations were previously unknown for this ligand.[37] Gratifyingly, the salt metathesis reaction of **1-Y** with one equivalent of KCp‴[38] in fluorobenzene proceeded at room temperature to give $[Y(Cp''')(Cp^*)(FPh)_2][\{Al[OC(CF_3)_3]_3\}_2(\mu\text{-F})]$ (**4-Y**) in a 57% yield following work-up and recrystallisation from a mixture of fluorobenzene and *n*-hexane (Fig. 1).

Bulk Solid-State Characterisation. Lower carbon values than expected were reproducibly obtained in elemental analysis results of **1-Ln** and **2-Ln**. This was ascribed to a combination of the experimental conditions employed and carbide formation,[39] which is particularly common for fluorine-rich complexes;[40] the lower than expected hydrogen values seen for **1-Y** was also

attributed to its high fluorine content. The other analytical data collected for **1-Ln** and **2-Ln** are in accord with the bulk purity of these samples. The ATR-IR spectra of **1-Ln** are essentially superimposable and are dominated by signals corresponding to the WCA (see Supporting Information Figs. S1 and S2). In contrast the ATR-IR spectra of **2-Dy** and **2-Y** are dissimilar due to the presence of crystals of **2-Dy·0.33$C_6H_5CH_3$** identified in batches of the former, but characteristic bridging and terminal B–H stretching modes could be assigned (see Supporting Information Figs. S3 and S4).[41] The ATR-IR spectrum of **4-Y** is unremarkable, with the majority of peaks being attributable to the WCA.

The DFT-calculated spectrum of **1-Y** shows that the expected C–F stretches (1106, 767 and 569 cm^{-1}) are all observed (see Supporting Information Fig. S6). The bulk phase purity of **1-Dy** was further demonstrated by powder XRD (see Supporting Information Figs. S7 and S8 and Table S2), as the diffraction pattern observed was in excellent agreement with that expected from single crystal XRD data (see below). Le Bail refinement gave reduced unit cell parameters, indicating that one molecule of hexane in the lattice per unit cell is lost upon preparation of samples of **1-Dy** for analysis; this could further account for the comparatively low carbon and hydrogen values obtained, but due to experimental uncertainties we do not adjust formula weights for the analysis of magnetic data (see below).

Solution Characterisation. Multinuclear NMR spectroscopic data was collected on solutions of **1-Ln**, **2-Ln** and **4-Y** (see Supporting Information Figs. S9–S19). Complexes **1-Ln** spontaneously form biphasic solutions in fluorobenzene, and this thwarted the collection of meaningful solution NMR data as other weakly coordinating polar solvents that can dissolve **1-Ln** including other halobenzenes will coordinate to the Ln(III) ions and displace the coordinated fluorobenzene.[27]

Attempts were made to collect NMR data on fluorobenzene solutions of **1-Ln** at elevated temperatures, but this led to sample decomposition.

The ^{1}H NMR spectrum of **2-Y** in C_6D_6 contains a singlet at 2.06 ppm integrating to 15H for the methyl groups, and a broad quartet at 0.66 ppm for the 8H corresponding to the borohydrides; the $^{13}C\{^{1}H\}$ NMR spectra also only shows two signals for the CH_3 (11.7 ppm) and quaternary C (123.5 ppm) environments, with no residual THF observed. The borohydride signal in the ^{1}H NMR spectrum is a broad quartet ($^{1}J_{BH}$ = 84.6 Hz) from coupling to 80.1% abundant I = 3/2 ^{11}B nuclei, with the coupling to 100% abundant I = 1/2 ^{89}Y nuclei not resolved; these assignments were confirmed by $^{1}H\{^{11}B\}$, $^{11}B\{^{1}H\}$ and ^{11}B NMR spectra, with the latter showing the expected pentet at –22.0 ppm from coupling to four ^{1}H nuclei. The NMR spectra of **2-Y** are comparable to those of $[Y(Cp^*)_2(\mu\text{-}BH_4)]_\infty$,[26] indicating that there is dynamic exchange on the NMR timescale. The paramagnetism of **2-Dy** precluded the observation of signals by ^{11}B, $^{11}B\{^{1}H\}$ and $^{13}C\{^{1}H\}$ NMR spectroscopy, whilst only one broad signal was observed in the ^{1}H NMR spectrum of a C_6D_6 solution at –57.65 ppm (FWHM ≈ 5,100 Hz) that we tentatively assign to the Cp* protons. The Evans method[42] was used to determine the magnetic susceptibility of **2-Dy** in C_6D_6 solution (10.46 μ_B), which is close to the expected value for a Dy(III) ion (10.50 μ_B).[43] The NMR data for **4-Y** are in accord with the expected spectra for this complex.

Single Crystal XRD. The solid-state structures of **1-Ln**, **2-Ln**, **3-Dy** and **4-Y** were determined by single crystal XRD (see Fig. 2 for depictions of the dication in **1-Dy** and the cation in **4-Y**; the structures of **1-Y**, **2-Ln** and **3-Dy** are compiled in the Supporting Information Figs. S20–S23, together with selected crystallographic parameters in Tables S3–S6). In the solid state the mono-ring complexes **2-Ln** are bridged by BH_4 groups to give oligomers that are comparable to

$[Y(Cp^*)_2(\mu\text{-}BH_4)]_\infty$;[27] hexameric **2-Dy·0.33C$_6$H$_5$CH$_3$** was also identified and the structure is reminiscent of $[La(Cp^{ttt})(\mu\text{-}BH_4)_2]_6$[44] and $[Ln(C_5Me_4{}^nPr)(\mu\text{-}BH_4)_2]_6$ (Ln = Nd, Sm).[45]

Despite the highly disordered WCAs in **1-Ln** giving inherently high R-factors for these datasets, the dications are relatively well-resolved, as are the lattice fluorobenzene and hexane molecules, with minimal structural disorder. The $[Ln(Cp^*)(FPh)_6]^{2+}$ dications in **1-Ln** exhibit six-legged piano stool geometries, with a Cp* "seat" and six monodentate fluorobenzene "legs" each binding *via* F lone pairs. These dications can alternatively be described as showing distorted *pseudo*-pentagonal bipyramidal geometries, with one F atom essentially *trans*- to the Cp* centroid ($Cp^*_{centroid}\cdots Dy–F$ = 176.20(9)°) and the five equatorial F atoms forming a plane with mean F–Dy–F angles of 69.65(4)°; the deviation from ideal 72° is due to the Dy atom being 0.570(2) Å above the F_5 plane. There is a wide range of $Cp^*_{centroid}\cdots Dy–F_{eq}$ (101.65(10)–106.54(14)°), F_{eq}–Dy–F_{eq} (73.94(12)–78.67(13)°), F_{eq}–Dy–F_{eq} (68.43(12)–70.8(2)°) and Dy–F–C_{ipso} (139.3(3)–166.6(4)°) angles in **1-Dy**, due to a combination of non-directional predominantly ionic bonding regimes and crystal packing effects.

The $Dy\cdots Cp^*_{centroid}$ distance (2.2737(4) Å) and mean Dy–F (2.402(2) Å) and F–C_{ipso} (1.420(3) Å) bond lengths of **1-Dy** are similar to those of the only two other structurally characterised fluorobenzene Dy complexes $[Dy(Cp^{ttt})(Cp^*)(FPh)][Al\{OC(CF_3)_3\}_4]$ ($Dy\cdots Cp^*_{centroid}$ = 2.315(2) Å; Dy–F = 2.429(2) Å; F–C_{ipso} = 1.414(4) Å)[27] and $[Dy(Cp^*)_2(FPh)_2][Al\{OC(CF_3)_3\}_4]$ (mean $Dy\cdots Cp^*_{centroid}$ = 2.286(2) Å; mean Dy–F = 2.358(12) Å; mean F–C_{ipso} = 1.42(3) Å).[26] The only previous structurally authenticated six-legged piano stool complex to our knowledge is $[Tm(Cp^*)(NCMe)_6][I]_2$,[30] which exhibits $Cp^*_{centroid}\cdots Tm–N$ (176.5(2)° for the axial NCMe; mean 102.5(2)° for the equatorial NCMe) and N–Tm–N (69.8(2)° mean between equatorial NCMe; 77.5(2)° between equatorial and axial NCMe) angles that are

comparable to the respective Cp*$_{centroid}$···Dy–F and F–Dy–F angles in **1-Dy**. Finally, the solid-state structure of the cation of **4-Y** is comparable to that seen in [Dy(Cp*)$_2$(FPh)$_2$][Al{OC(CF$_3$)$_3$}$_4$], albeit with longer Ln···Cp$^R_{centroid}$ distances (Y···Cp‴$_{centroid}$: 2.3100(4) Å; Y···Cp*$_{centroid}$: 2.3703(4) Å; Dy···Cp*$_{centroid}$: 2.2763(8) and 2.2957(7) Å) and a more bent Cp$^R_{centroid}$···Ln···Cp$^R_{centroid}$ geometry (**4-Y**: 138.49(2)°; [Dy(Cp*)$_2$(FPh)$_2$][Al{OC(CF$_3$)$_3$}$_4$]: 142.49(4)°).[26]

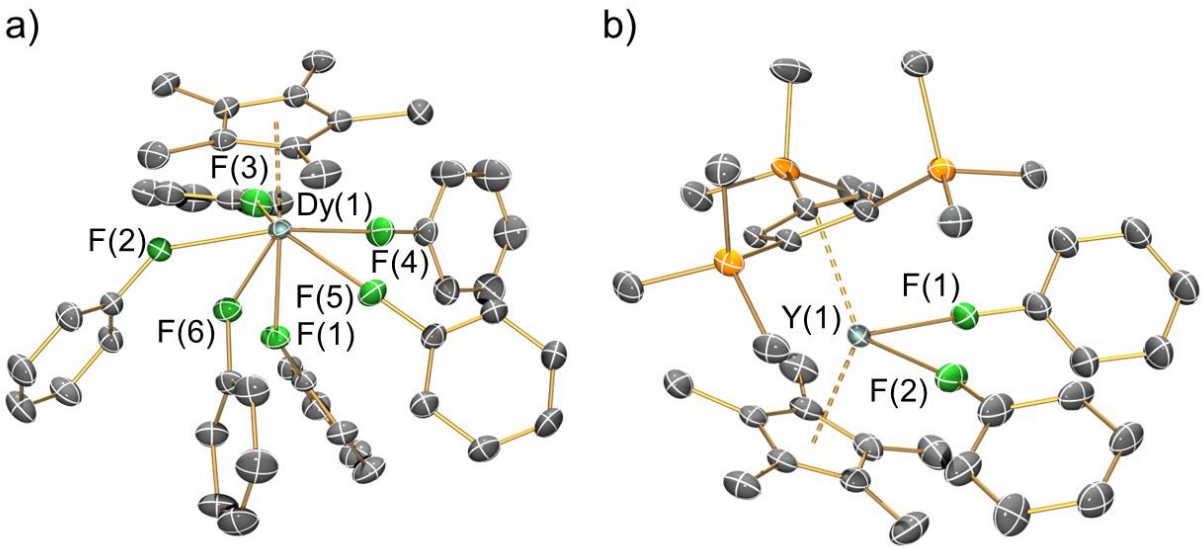

Fig. 2. Single crystal XRD structures of a) the dication of **1-Dy** and b) the cation of **4-Y** with selected atom labelling (Y/Dy: cyan, C: grey, F: green, Si: orange). Displacement ellipsoids set at 20% probability levels; hydrogen atoms, the lattice solvents and the counteranions have been omitted for clarity. See Supporting Information for selected bond lengths and angles.

Magnetism. The static and dynamic magnetic properties of polycrystalline **1-Dy** in the solid-state were determined by SQUID magnetometry (see Supporting Information Figs. S25–S29 and Tables S7 and S8). The molar magnetic susceptibility-temperature product χT is 14.0 cm^3 K mol^{-1} at room

temperature, similar to that predicted for a free Dy(III) ion ($^6H_{15/2}$, χT = 14.2 cm^3 K mol^{-1})[43] and the CASSCF-SO-calculated value (see Supporting Information Fig. S25). There is minimal variation in χT with temperature until 13 K, at which point a sharp decline is observed that is typical of magnetic blocking. Open magnetic hysteresis loops are present at 2 K and remain open up to T_H = 14 K at a sweep rate of 22 Oe s^{-1} in the zero-field region (Fig. 3), with a large drop at zero-field indicating efficient QTM. It is remarkable that **1-Dy** with only one anionic ligand has similar T_H to the best-performing *bis*-Cp* Dy(III) SMMs with weak equatorial ligands, e.g. [{Dy(Cp*)$_2$(μ-(Me)$_2$AlMeNEt$_3$)}$_2$][Al{OC(CF$_3$)$_3$}$_4$]$_2$ (12 K)[25] and [Dy(Cp*)$_2$(XPh)$_2$][Al{OC(CF$_3$)$_3$}$_4$] (X = F, 8 K; X = Cl, 10 K).[26] We posit that the comparable relaxation dynamics of **1-Dy** to these literature examples is due to its $\pm m_J$ states being more pure from not having a second anionic ligand introducing strong transverse fields, despite the smaller axial crystal field (CF) imposed by only one Cp* ligand (see below).

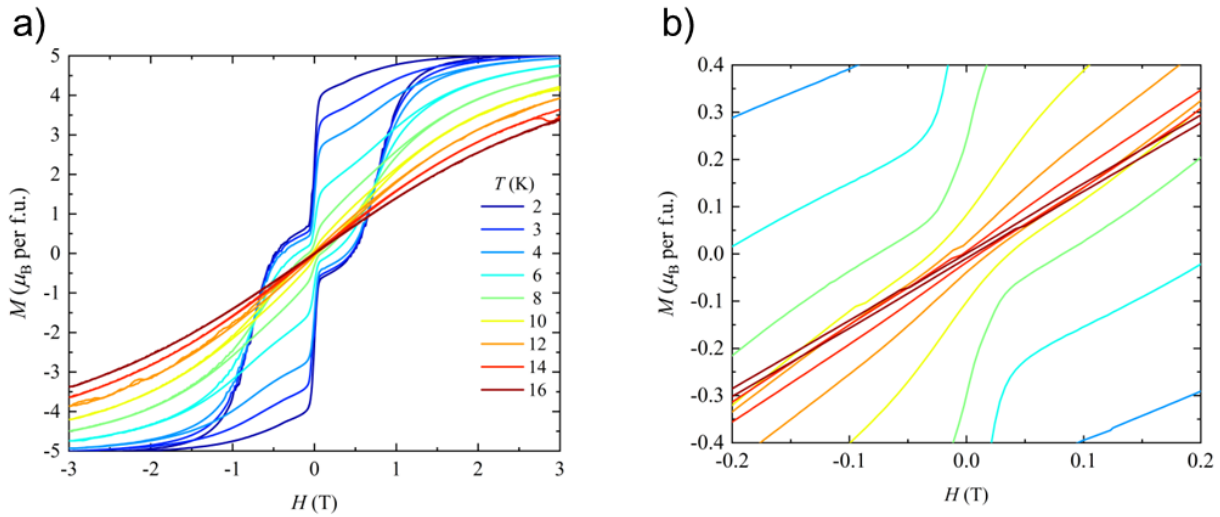

Fig. 3. a) Hysteresis loops of **1-Dy** from 2 to 20 K and –3 T to +3 T, sweep rate is 22 Oe s^{-1}. b) Hysteresis loops of **1-Dy** at 4–16 K between –3 and +3 T zoomed in between –0.2 and +0.2 T, sweep rate is 22 Oe s^{-1}. Hysteresis is considered open until T_H = 14 K.

Peaks were observed in zero-field AC susceptibility data for **1-Dy** at temperatures between 18–52.5 K, and these data fitted well to generalized Debye models (fit with CC-FIT2,[46,47] see Supporting Information Fig. S26 and S27 and Table S7). To determine the low temperature relaxation dynamics, magnetisation decay measurements of **1-Dy** were performed in zero field between 2–12 K (see Supporting Information Figs. S28 and S29). The decays at T ≤ 10 K clearly indicate two different relaxation timescales in **1-Dy**, necessitating a double stretched exponential model (Equation S2),[48] while data at T = 12 K exhibits only single stretched exponential decay (Equation S3). The relaxation profile of **1-Dy** (Fig. 4) shows clear exponential Orbach relaxation at high-temperatures, switching to a power-law Raman process below τ_{switch} = 39 K.[49] At low temperatures, there are two clear relaxation processes: one with faster rates showing temperature-independent relaxation dynamics indicative of QTM, and one with slower rates that follows the higher-temperature Raman profile. The fraction of the two processes is approximately 50 : 50 at the lowest temperatures, with the faster component becoming more dominant as the temperature increases (Supporting Information Table S8). The relaxation profile was globally fitted to a model with Orbach ($10^{-A}e^{\frac{U_{\text{eff}}}{T}}$), Raman ($10^{R}T^{n}$) and QTM ($10^{-Q}$) contributions (Equation S4), with no QTM contribution to the slow DC decay rates. The resulting fitted parameters are U_{eff} = 564(33) cm^{-1}, A = –10.37(43) log$_{10}$[s], R = –6.08(9) log$_{10}$ [s^{-1} K^{n}], n = 4.67(8) and Q = 0.814(25) log$_{10}$ [s], with the model and experimental data in good agreement.

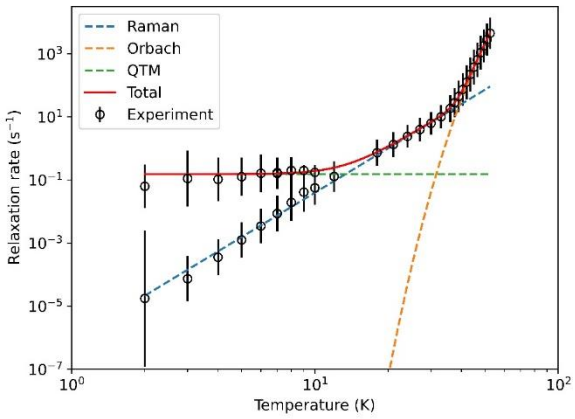

Fig. 4. Fitting of **1-Dy** relaxation profile, showing Orbach, Raman and QTM components derived with Equation S4. Error bars represent one ESD in the distribution of rates.

***Ab Initio* Calculations.** CASSCF-SO calculations were performed on molecular structures obtained from single crystal XRD studies (see Supporting Information for details). We approximate a calculated U_{eff} for the dication of **1-Dy** as the energy of the first Kramers doublet with significant transverse g_x and/or g_y values (> 1), giving 589 cm^{-1} at the 5th excited state (Fig. 5 and Table S9), which is in excellent agreement with the measured data. The ground state g_z value is aligned along $Cp^*_{centroid}\cdots Dy–F_{ax}$, and the CF states up to the 5th excited state are essentially pure $\pm m_J$ functions due to the lack of strong off-axis interactions and the relatively symmetrical distribution of the five equatorially-bound fluorobenzenes, such that their contribution to the anisotropy axis cancels;[50,51] the retention of purity is reminiscent of the predicted electronic structure of the theoretical $[DyO]^+$ cation.[6] It is noteworthy that the U_{eff} and T_H of **1-Dy** are similar to the range of values (U_{eff} = 354(34)–453(72) cm^{-1} and T_H = 9–11 K) observed for the distorted pentagonal bipyramidal Dy(III) complexes $[Dy(OR)(X)(THF)_5][BPh_4]$ (R = CMe_3, $SiMe_3$, Ph; X

= Cl, Br), but in those cases Orbach magnetic relaxation proceeds *via* only the second excited state,[52] versus the 5th excited state here.

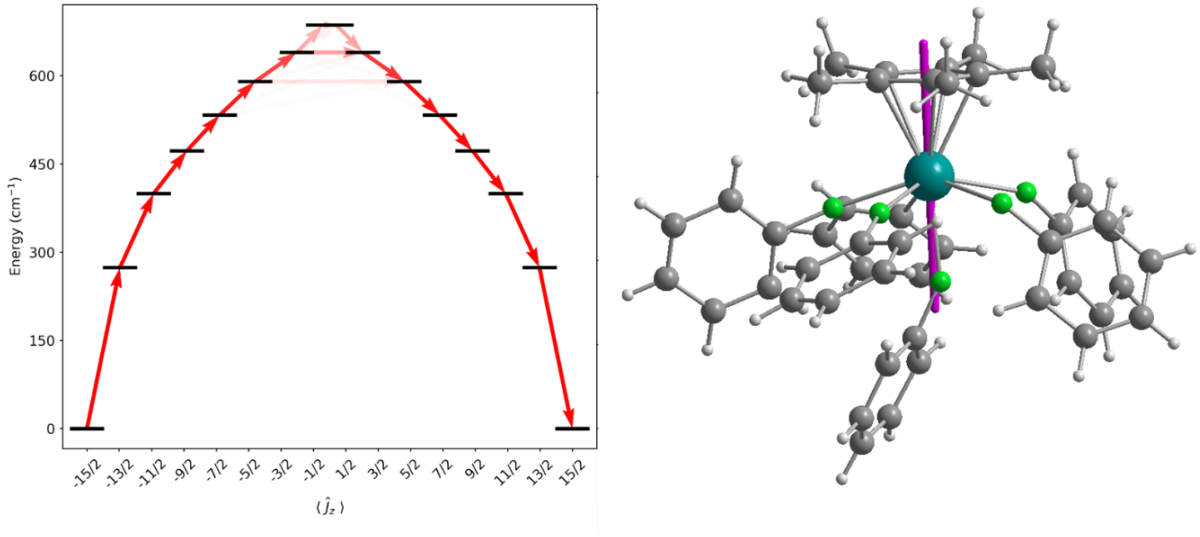

Fig. 5. Energy barrier to magnetic relaxation for a model of $[Dy(Cp^*)(FPh)_6]^{2+}$. Electronic states from CASSCF-SO calculations, labelled with their dominant m_J composition in the J = 15/2 basis. Arrows represent the Orbach relaxation pathway, where the opacity of the arrows is proportional to the transition probability approximated with the average matrix elements of magnetic moment connecting the states, $\gamma_{ij} = (1/3)[|\langle i|\mu_x|j\rangle|^2 + |\langle i|\mu_y|j\rangle|^2 + |\langle i|\mu_z|j\rangle|^2]$, normalized from each departing state and commencing from |–15/2> (left). Denotation of the g_z axis (purple) within the solid-state structure at the ground state (right).

To understand how the fluorobenzene ligands affect the magnetic anisotropy of **1-Dy**, we performed CASSCF-SO calculations on model complexes using the metrical parameters from the single crystal XRD structure of **1-Dy** as a starting point (see Supporting Information Figs. S30–S33 and Tables S9–S13). The calculated U_{eff} values of hypothetical $[Dy(Cp^*)]^{2+}$ and

$[Dy(Cp^*)(FPh)]^{2+}$ dications, with only the axially-bound fluorobenzene retained in the latter, are 1071 cm^{-1} and 1505 cm^{-1}, respectively. This highlights the constructive role of the axially-bound *trans*-fluorobenzene ligand that can vastly increase U_{eff} *c.f.* $[Dy(Cp^*)]^{2+}$, as well as the destructive role of the equatorial fluorobenzene ligands that reduce U_{eff} down to 589 cm^{-1}. While these significant changes in U_{eff} with different dispositions of neutral solvent molecules clearly demonstrates the shortcomings of the classical electrostatic model, the observation that the equatorial neutral solvent molecules do not significantly mix the $\pm m_J$ states is remarkable.[51] Although the $[Dy\{OC(CF_3)_3\}_2(FPh)_5]^+$ cation of **3-Dy** contains weakly-bound fluorinated alkoxides, its predicted U_{eff} value (1275 cm^{-1}) is competitive with many axial Dy(III) alk/aryloxide SMMs with more strongly donating axial and equatorial ligands[53] (current record U_{eff} = 1687 cm^{-1} for $[Dy(OAd)_2(18\text{-crown-6})][I_3]$),[54] thus the deliberate synthesis of haloarene analogues of ether- and pyridine-bound axial Dy alk/aryloxide complexes should also be worthwhile targets for the SMM community. Finally, the U_{eff} value for the $[Y(Cp''')(Cp^*)(FPh)_2]^+$ cation in **4-Y** is predicted to be 674 cm^{-1}, due to a combination of its bent $Cp'''_{centroid}\cdots Y\cdots Cp^*_{centroid}$ motif and equatorially-bound fluorobenzenes; the Dy analogue was not targeted as it would not give notable SMM properties compared to other leading Dy(III) *bis*-Cp^R SMMs.[13–16,27]

To summarise, we have synthesised and characterised a new class of Ln SMM, where the magnetic anisotropy and resultant magnetic properties are dominated by only one anionic ligand. A relatively modest U_{eff} value is found for **1-Dy** as it only possesses one anionic Cp* ligand in the six-legged piano stool Dy(III) dication $[Dy(Cp^*)(FPh)_6]^{2+}$. *Ab initio* studies of theoretical $[Dy(Cp^*)]^{2+}$ and $[Dy(Cp^*)(FPh)]^{2+}$ dications revealed that the U_{eff} of **1-Dy** is enhanced by the axial fluorobenzene and diminished by the equatorial fluorobenzenes, but, crucially, the transverse CF introduced by the five equatorially-bound fluorobenzenes is weak and the $\pm m_J$ states maintain high

purity. As a result, **1-Dy** shows open magnetic hysteresis up to 14 K, which is comparable to the best-performing Dy(III) *bis*-Cp* complexes reported to date.[25,26,55–57] We have also demonstrated the facile displacement of fluorobenzene from **1-Y** in a salt metathesis reaction to give a Ln metallocenium cation, $[Y(Cp''')(Cp^*)(FPh)_2]^+$, that could not be isolated by standard abstraction methodologies. We envisage that extending the synthetic methods herein to a wider range of $[Ln(L)(XPh)_n]^{2+}$ dications (L = anionic ligand, X = halogen) will provide complexes with interesting properties, which can be exploited as useful starting materials to hitherto unknown heteroleptic Ln complexes, including high temperature Ln SMMs.

Methods

General. All manipulations were performed in an inert argon atmosphere with rigorous exclusion of oxygen and water using Schlenk line and glovebox techniques. The solvents *n*-hexane, toluene and benzene were dried by refluxing over potassium and stored over potassium mirrors. Pentane was dried by refluxing over NaK and stored over a potassium mirror. Fluorobenzene and *ortho*-difluorobenzene were dried by refluxing over CaH_2 and was stored over 4 Å molecular sieves. Tetrahydrofuran (THF) was dried by refluxing over potassium and stored over 4 Å molecular sieves. All solvents were degassed before use. The starting materials $[Y(BH_4)_3(THF)_3]$,[32] $[Dy(BH_4)_3(THF)_3]$,[32] KCp*,[33] KCp'''[38] and PhF-Al{$OC(CF_3)_3$}$_3$[58] were prepared according to literature methods. $[CPh_3][\{Al[OC(CF_3)_3]_3\}_2(\mu\text{-F})]$ was synthesised by a modification of the published procedure.[34] The reagent $[CPh_3][PF_6]$ was purchased from Sigma-Aldrich and was used as received.

^{1}H (400 MHz), ^{13}C (126 MHz), ^{11}B (128 MHz),^{19}F (376 MHz) and ^{29}Si DEPT90 (80 MHz) NMR spectra were obtained on a Bruker Avance III 400 or 500 MHz spectrometer at 298 K and

were referenced to the solvent used, or to external $SiMe_4$ (^1H, ^{13}C, ^{29}Si), H_3BO_3/D_2O (^{11}B) or $C_7H_5F_3/CDCl_3$ (^{19}F). ATR-IR spectra were recorded on a Bruker Alpha spectrometer with Platinum-ATR module. Elemental analysis was carried out by Mr Martin Jennings and Mrs Anne Davies at the Microanalytical service, Department of Chemistry, the University of Manchester. NMR and ATR-IR spectra are compiled in the Supporting Information, together with details of single crystal and powder XRD, SQUID magnetometry, and DFT and CASSCF-SO calculations.

Preparation of $[Y(Cp^*)(FPh)_6][\{Al[OC(CF_3)_3]_3\}_2(\mu\text{-}F)]_2$ (1-Y). Fluorobenzene (30 mL) was added to a mixture of **2-Y** (0.508 g, 2.0 mmol) and $[CPh_3][\{Al[OC(CF_3)_3]_3\}_2(\mu\text{-}F)]$ (6.906 g, 4.0 mmol). The reaction mixture was heated to 70 °C and stirred for 30 min. The solution was concentrated *in vacuo* to 5 mL; *n*-hexane (50 mL) was then added, and the mixture vigorously stirred to form a yellow oil. The supernatant was decanted and fluorobenzene (30 mL) was added to the crude product; the mixture was stirred for 10 min. The product collected as the bottom layer of a biphasic solution; the top layer was decanted, and the addition of fluorobenzene and separation of the layers was repeated. The remaining yellow solution was layered with *n*-hexane (30 mL) and stored at room temperature to give bright yellow crystals. The supernatant was decanted, and residual solvent removed to give **1-Y** (5.002 g, 1.3 mmol, 64%). Anal. Calcd for $C_{206}H_{123}Al_8F_{233}O_{24}Y_2$: C, 31.71; H, 1.59. Found: C, 29.23; H, 0.96. The formation of biphasic solutions in fluorobenzene together with rapid fluorobenzene exchange dynamics precluded the collection of meaningful solution NMR data. FTIR (ATR, microcrystalline): $\tilde{\nu}$ = 2964 (w, C–H stretch), 2875 (w, C–H stretch), 1585 (w), 1486 (m), 1453 (w), 1354 (m, C–O stretch), 1301 (s), 1274 (s, C–F stretch), 1239 (s), 1211 (s), 1174 (s), 1116 (m), 1106 (s, C–F stretch), 1067 (w), 1019

(w), 970 (s), 896 (w), 863 (m), 808 (w), 767 (m, C–F stretch), 748 (s), 725 (s), 705 (w), 674 (w), 635 (m), 569 (m, C–F stretch), 536 (s), 471 (w), 450 (s) cm^{-1}.

Preparation of $[Dy(Cp^*)(FPh)_6][\{Al[OC(CF_3)_3]_3\}_2(\mu\text{-}F)]_2$ (1-Dy). Complex **1-Dy** was prepared following analogous synthetic and work-up procedures to **1-Y** from **2-Dy** (0.537 g, 1.5 mmol) and $[CPh_3][\{Al[OC(CF_3)_3]_3\}_2(\mu\text{-}F)]$ (5.179 g, 3.0 mmol). The product **1-Dy** was isolated as orange crystals (2.273 g, 0.6 mmol). A second crop of **1-Dy** was obtained from the combined fluorobenzene supernatant solutions (1.162 g, 0.3 mmol). Total yield = 3.435 g, 0.9 mmol, 58%. Anal. Calcd for $C_{206}H_{123}Al_8Dy_2F_{233}O_{24}$: C, 31.12; H, 1.56. Found: C, 28.61; H, 1.33. The formation of biphasic solutions in fluorobenzene together with rapid fluorobenzene exchange dynamics and the paramagnetism of **1-Dy** precluded the collection of meaningful solution NMR data. FTIR (ATR, microcrystalline): $\tilde{\nu}$ = 2955 (w, C–H stretch), 2929 (w, C–H stretch), 1585 (w), 1486 (m), 1453 (w), 1354 (m, C–O stretch), 1301 (s), 1268 (s, C–F stretch), 1241 (s), 1211 (s), 1176 (s), 1118 (m), 1108 (s, C–F stretch), 1067 (w), 1019 (w), 970 (s), 896 (w), 861 (m), 834 (w), 808 (w), 769 (m, C–F stretch), 748 (s), 725 (s), 705 (w), 676 (w), 635 (m), 569 (m, C–F stretch), 536 (s), 485 (w), 450 (s) cm^{-1}.

Preparation of $[Y(Cp^*)(BH_4)_2]_\infty$ (2-Y). THF (40 mL) was added to a mixture of $[Y(BH_4)_3(THF)_3]$ (2.099 g, 6.0 mmol) and KCp* (1.046 g, 6.0 mmol), and the reaction mixture was stirred at room temperature for 48 h. Following the removal of THF under vacuum, toluene (40 mL) was used to extract the crude product, and filtration gave a colourless solution. The solvent was removed *in vacuo* to give a colourless oil, which was heated (150 °C) under vacuum (10^{-3} mbar) for 6 h. Hot toluene (50 mL) was used to extract the product, which was filtered. The solvent

was removed under vacuum and the product dissolved in benzene (30 mL) and stored at 6 °C to afford colourless crystals. The supernatant was decanted, and the residual solvent was removed *in vacuo* to give **2-Y** (0.865 g, 3.4 mmol). The supernatant was concentrated under vacuum to *ca*. 10 mL to yield an additional crop of **2-Y** as colourless microcrystals (0.254 g, 1.0 mmol). Total yield = 1.119 g, 4.4 mmol, 73 %. Anal. Calcd for $C_{10}H_{23}B_2Y$: C, 47.32; H, 9.13. Found: C, 47.00; H, 9.18. ^{1}H NMR (400.13 MHz, C_6D_6, 298 K): δ = 2.06 (s, 15H, Cp-C(C*H*$_3$)), 0.66 (br q, 8H, $^1J_{BH}$ = 84.6 Hz, BH_4). $^{13}C\{^1H\}$ NMR (125.79 MHz, C_6D_6, 298 K): δ = 123.5 (Cp-*C*(CH_3)), 11.7 (Cp-C(*C*H_3)). $^{11}B\{^1H\}$ NMR (160.48 MHz, C_6D_6, 298 K): δ = –22.0 (*B*H_4). ^{11}B NMR (128.38 MHz, C_6D_6, 298 K): δ = –22.0 (p, $^1J_{BH}$ = 84.6 Hz, *B*H_4). FTIR (ATR, microcrystalline): $\tilde{\nu}$ = 2970 (w, C–H stretch), 2941 (w, C–H stretch), 2910 (m, C–H stretch), 2859 (m, C–H stretch), 2499 (s, B–H_t stretch), 2277 (s, B–H_b stretch), 2203 (s, B–H_b stretch), 2133 (s, B–H_b stretch), 1485 (w), 1455 (w), 1432 (w), 1381 (w), 1204 (s), 1116 (s), 1093 (m), 1026 (m), 802 (w), 676 (w), 592 (w), 434 (s) cm^{-1}.

Preparation of [Dy(Cp*)(BH$_4$)$_2$]$_\infty$ (2-Dy). Complex **2-Dy** was prepared following analogous synthetic procedures to **2-Y** from [Dy(BH_4)$_3$(THF)$_3$] (2.117 g, 5.0 mmol) and KCp* (0.872 g, 5.0 mmol). The product was crystallised from toluene (10 mL) as bright yellow crystals after storage at –35 °C. The supernatant was decanted, and residual solvent removed *in vacuo* to afford **2-Dy** (1.138 g, 3.2 mmol, 64%). A hexameric form that contains two lattice toluene molecules (**2-Dy·0.33C$_6$H$_5$CH$_3$**) was also identified in this crop by single crystal XRD. Anal. Calcd for $C_{10}H_{23}B_2Dy$: C, 36.68; H, 7.08. Found: C, 35.45; H, 7.32. μ_{eff} product = 10.46 μ_B (Evans method, C_6D_6, 298 K). The paramagnetism of **2-Dy** precluded the assignment of its ^{1}H, $^{13}C\{^1H\}$ and $^{11}B\{^1H\}$ NMR spectra. FTIR (ATR, microcrystalline): $\tilde{\nu}$ = 2959 (w, C–H stretch), 2945 (w, C–H

stretch), 2908 (m, C–H stretch), 2859 (m, C–H stretch), 2491 (s, B–H_t stretch), 2277 (s, B–H_b stretch), 2216 (m, B–H_b stretch), 2127 (s, B–H_b stretch), 1490 (w), 1451 (w), 1432 (w), 1379 (w), 1300 (w), 1262 (m), 1214(m), 1196 (s), 1114 (m), 1097 (s), 1023 (s), 863 (w), 802 (m), 730 (m), 694 (w), 590 (w), 464 (w) cm^{-1}.

Preparation of [Dy{OC(CF$_3$)$_3$}$_2$(FPh)$_5$][{Al[OC(CF$_3$)$_3$]$_3$}$_2$(μ-F)] (3-Dy). Fluorobenzene (5 mL) was added to a mixture of **2-Dy** (0.107 g, 0.3 mmol) and [CPh$_3$][Al{OC(CF$_3$)$_3$}$_4$] (0.726 g, 0.6 mmol) at room temperature. The reaction mixture was heated to 70 °C for 30 minutes, the solvent was removed *in vacuo* and the resultant yellow oil washed with hexane (5 mL). The crude product was dissolved in fluorobenzene (1 mL) and layered with hexane (5 mL) to give several crystals of **3-Dy**.

Preparation of [Y(Cp‴)(Cp*)(FPh)$_2$][{Al[OC(CF$_3$)$_3$]$_3$}$_2$(μ-F)] (4-Y). Fluorobenzene (10 mL) was added to a mixture of **1-Y** (0.948 g, 0.25 mmol) and KCp‴ (0.080 g, 0.25 mmol). The yellow reaction mixture was stirred at room temperature for 7 days. The solution was concentrated *in vacuo* to *ca*. 5 mL; *n*-hexane (5 mL) was then added, and the mixture was vigorously stirred to form a light yellow solution and an off-white solid. The supernatant was separated by filtration and concentrated *in vacuo* to *ca*. 4 mL; the mixture was stored at –35 °C for 3 days to afford light yellow crystals. The supernatant was decanted, and the residual solvent was removed under vacuum to give **4-Y** (0.312 g, 0.17 mmol, 57%). Anal. Calcd for $C_{60}H_{54}Al_2F_{57}O_6Si_3Y$: C, 33.04; H, 2.50. Found: C, 31.46; H, 2.21. ^{1}H NMR (400.13 MHz, C_6H_5F with a C_6D_6/C_6H_5F insert, 298 K): δ = 7.45 (s, 2H, Cp-C*H*), 1.90 (s, 15H, Cp-CH_3), 0.30 (s, 9H, Si(CH_3)$_3$), 0.26 (s, 18H, Si(CH_3)$_3$). ^{13}C{^{1}H} NMR (125.79 MHz, C_6H_5F with a C_6D_6/C_6H_5F insert, 298 K): δ = 141.1 (Cp-

*C*Si(CH_3)$_3$), 140.3 (Cp-*C*H), 134.6 (Cp-*C*Si(CH_3)$_3$), 125.8 (Cp-*C*(CH_3), 11.5 (Cp-C(*C*H_3)) 1.0 (Si(*C*H_3)$_3$), 0.3 (Si(*C*H_3)$_3$). ^{19}F NMR (376.46 MHz, C_6H_5F with a C_6D_6/C_6H_5F insert, 298 K): δ = –75.4 (s, [{Al[OC(C*F*$_3$)$_3$]$_3$}$_2$(*μ*-F)]), –113.7 (br. s, C_6H_5*F*), –184.5 (s, [{Al[OC(CF_3)$_3$]$_3$}$_2$(*μ*-*F*)]). ^{29}Si DEPT90 NMR (80 MHz, C_6H_5F with a C_6D_6/C_6H_5F insert, 298 K): δ = –8.37 (*Si*(CH_3)$_3$), –8.64 (*Si*(CH_3)$_3$). FTIR (ATR, microcrystalline): $\tilde{\nu}$ = 2961 (w, C–H stretch), 2923 (w, C–H stretch), 1580 (w), 1484 (m), 1354 (m, C–O stretch), 1301 (s), 1276 (s, C–F stretch), 1241 (s), 1215 (s), 1169 (s), 1114 (m), 1087 (m), 1069 (w), 1019 (w), 972 (s), 935 (m), 896 (w), 859 (m), 834 (s), 773 (m), 752 (s), 725 (s), 705 (w), 676 (w), 633 (s), 569 (m), 536 (s), 507 (w), 483 (w), 450 (s), 425 (m) cm^{-1}.

[CPh$_3$][{Al[OC(CF$_3$)$_3$]$_3$}$_2$(*μ*-F)]. Prepared by a modification of the published procedure.[34] *Ortho*-difluorobenzene (50 mL) was added to a mixture of [CPh$_3$][PF$_6$] (3.657 g, 9.4 mmol) and PhF-Al{OC(CF_3)$_3$}$_3$ (15.604 g, 18.8 mmol); an immediate effervescence and formation of a dark yellow solution was observed. The reaction mixture was stirred at room temperature for 16 h. The solvent was removed *in vacuo*, and the remaining solid washed with pentane (3 × 30 mL). The residual solvent was removed under vacuum and the product was obtained as a bright yellow powder (15.537 g, 9.0 mmol, 96%). The identity of the product was confirmed by comparison to literature NMR spectroscopic data.

Data availability

Supplementary information is available in the online version of the paper. Reprints and permissions information is available online at www.nature.com/reprints. Correspondence and requests for materials should be directed to N.F.C. and D.P.M. Crystallographic data for the

structures reported in this Article have been deposited at the Cambridge Crystallographic Data Centre, under deposition numbers CCDC 2365779 (**1-Y**), 2365780 (**1-Dy**), 2365781 (**2-Y**), 2365782 (**2-Dy**), 2365783 (**2-Dy·0.33$C_6H_5CH_3$**), 2365784 (**3-Dy**), 2365785 (**4-Y**). Copies of the data can be obtained free of charge from the CCDC via www.ccdc.cam.ac.uk/getstructures. Raw research data files supporting this publication are available from Figshare at https://doi.org/10.6084/m9.figshare.26105386. Apart from the data sets mentioned, all other data supporting the findings of this study are available within the Article and Supplementary information.

References

1. Gatteschi, D., Sessoli, R. & Villain, J. *Molecular Nanomagnets*. (Oxford University Press, 2006). doi:10.1093/acprof:oso/9780198567530.001.0001.
2. Ishikawa, N., Sugita, M., Ishikawa, T., Koshihara, S. Y. & Kaizu, Y. Lanthanide double-decker complexes functioning as magnets at the single-molecular level. *J. Am. Chem. Soc.* **125**, 8694–8695 (2003).
3. Clemente-Juan, J. M., Coronado, E. & Gaita-Ariño, A. Mononuclear Lanthanide Complexes: Use of the Crystal Field Theory to Design Single-Ion Magnets and Spin Qubits. in *Lanthanides and Actinides in Molecular Magnetism* 27–60 (Wiley, 2015). doi:10.1002/9783527673476.ch2.
4. Giansiracusa, M. J., Gransbury, G. K., Chilton, N. F. & Mills, D. P. Single-Molecule Magnets. in *Encyclopedia of Inorganic and Bioinorganic Chemistry* 1–21 (John Wiley & Sons Ltd, 2021). doi:10.1002/9781119951438.eibc2784.
5. Rinehart, J. D. & Long, J. R. Exploiting single-ion anisotropy in the design of f-element

single-molecule magnets. *Chem. Sci.* **2**, 2078–2085 (2011).

6. Ungur, L. & Chibotaru, L. F. Magnetic anisotropy in the excited states of low symmetry lanthanide complexes. *Phys. Chem. Chem. Phys.* **13**, 20086–20090 (2011).
7. Chilton, N. F., Goodwin, C. A. P., Mills, D. P. & Winpenny, R. E. P. The first near-linear bis(amide) f-block complex: A blueprint for a high temperature single molecule magnet. *Chem. Commun.* **51**, 101–103 (2015).
8. Ortu, F. & Mills, D. P. Low-coordinate rare-earth and actinide complexes. in *Handbook on the Physics and Chemistry of Rare Earths* (eds. Bünzli, J.-C. G. & Pecharsky, V. K.) vol. 55 1–87 (Elsevier B.V., 2019).
9. Yang, W. *et al.* Single Molecule Magnetism with Strong Magnetic Anisotropy and Enhanced Dy···Dy Coupling in Three Isomers of Dy-Oxide Clusterfullerene $Dy_2O@C_{82}$. *Adv. Sci.* **6**, 1901352 (1–18) (2019).
10. Velkos, G. *et al.* Shape-adaptive single-molecule magnetism and hysteresis up to 14 K in oxide clusterfullerenes $Dy_2O@C_{72}$ and $Dy_2O@C_{74}$ with fused pentagon pairs and flexible Dy–(μ_2-O)–Dy angle. *Chem. Sci.* **11**, 4766–4772 (2020).
11. Velkos, G. *et al.* Metallofullerene single-molecule magnet $Dy_2O@C_{2v}(5)$-C_{80} with a strong antiferromagnetic Dy···Dy coupling. *Chem. Commun.* **58**, 7164–7167 (2022).
12. Yang, W. *et al.* Carbon cage isomers and magnetic Dy···Dy interactions in $Dy_2O@C_{88}$ and $Dy_2C_2@C_{88}$ metallofullerenes. *Inorg. Chem. Front.* **9**, 5805–5819 (2022).
13. Goodwin, C. A. P., Ortu, F., Reta, D., Chilton, N. F. & Mills, D. P. Molecular magnetic hysteresis at 60 kelvin in dysprosocenium. *Nature* **548**, 439–442 (2017).
14. McClain, K. R. *et al.* High-temperature magnetic blocking and magneto-structural correlations in a series of dysprosium(III) metallocenium single-molecule magnets. *Chem.*

Sci. **9**, 8492–8503 (2018).

15. Guo, F. S. *et al.* Magnetic hysteresis up to 80 kelvin in a dysprosium metallocene single-molecule magnet. *Science* **362**, 1400–1403 (2018).

16. Gransbury, G. K. *et al. AtomAccess*: A Predictive Tool for Molecular Design and Its Application to the Targeted Synthesis of Dysprosium Single-Molecule Magnets. *J. Am. Chem. Soc.* **145**, 22814–22825 (2023).

17. Evans, P., Reta, D., Whitehead, G. F. S., Chilton, N. F. & Mills, D. P. Bis-monophospholyl dysprosium cation showing magnetic hysteresis at 48 K. *J. Am. Chem. Soc.* **141**, 19935–19940 (2019).

18. Guo, F.-S. *et al.* Discovery of a Dysprosium Metallocene Single-Molecule Magnet with Two High-Temperature Orbach Processes. *Inorg. Chem.* **61**, 6017–6025 (2022).

19. Vanjak, J. C. *et al.* A High-Performance Single-Molecule Magnet Utilizing Dianionic Aminoborolide Ligands. *J. Am. Chem. Soc.* **144**, 17743–17747 (2022).

20. Vincent, A. H., Whyatt, Y. L., Chilton, N. F. & Long, J. R. Strong Axiality in a Dysprosium(III) Bis(borolide) Complex Leads to Magnetic Blocking at 65 K. *J. Am. Chem. Soc.* **145**, 1572–1579 (2023).

21. Gould, C. A. *et al.* Synthesis and Magnetism of Neutral, Linear Metallocene Complexes of Terbium(II) and Dysprosium(II). *J. Am. Chem. Soc.* **141**, 12967–12973 (2019).

22. Gould, C. A. *et al.* Ultrahard magnetism from mixed-valence dilanthanide complexes with metal-metal bonding. *Science* **375**, 198–202 (2022).

23. Staab, J. K., Rahman, M. K. & Chilton, N. F. Intramolecular bridging strategies to suppress two-phonon Raman spin relaxation in dysprosocenium single-molecule magnets. *Phys. Chem. Chem. Phys.* (2024) doi:10.1039/D4CP01716A.

24. Reta, D., Kragskow, J. G. C. & Chilton, N. F. Ab Initio Prediction of High-Temperature Magnetic Relaxation Rates in Single-Molecule Magnets. *J. Am. Chem. Soc.* **143**, 5943–5950 (2021).

25. Evans, P. *et al.* A double-dysprosocenium single-molecule magnet bound together with neutral ligands. *Chem. Commun.* **56**, 5677–5680 (2020).

26. Corner, S. C. *et al.* Synthesis and Magnetic Properties of Bis-Halobenzene Decamethyldysprosocenium Cations. *Inorg. Chem.* **63**, 9562–9571 (2024).

27. Corner, S. C. *et al.* Halobenzene Adducts of a Dysprosocenium Single-Molecule Magnet. *Inorg. Chem.* **63**, 9552–9561 (2024).

28. Arndt, S. & Okuda, J. Cationic Alkyl Complexes of the Rare-Earth Metals: Synthesis, Structure, and Reactivity. *Adv. Synth. Catal.* **347**, 339–354 (2005).

29. Arndt, S. & Okuda, J. Mono(cyclopentadienyl) Complexes of the Rare-Earth Metals. *Chem. Rev.* **102**, 1953–1976 (2002).

30. Evans, W. J. *et al.* Structural studies of mono(pentamethylcyclopentadienyl)lanthanide complexes. *J. Coord. Chem.* **59**, 1069–1087 (2006).

31. Pike, S. D., Crimmin, M. R. & Chaplin, A. B. Organometallic chemistry using partially fluorinated benzenes. *Chem. Commun.* **53**, 3615–3633 (2017).

32. Goodwin, C. A. P. *et al.* Terbocenium: Completing a heavy lanthanide metallocenium cation family with an alternative anion abstraction strategy. *Chem. Commun.* **54**, 9182–9185 (2018).

33. Rabe, G., Roesky, H. W., Stalke, D., Pauer, F. & Sheldrick, G. M. The preparation and crystal structures of sodium and potassium pentamethylcyclopentadienyl pyridine solvates. *J. Organomet. Chem.* **403**, 11–19 (1991).

34. Martens, A. *et al.* Facile and systematic access to the least-coordinating WCA $[(R^FO)_3Al–F–Al(OR^F)_3]^-$ and its more Lewis-basic brother $[F–Al(OR^F)_3] - (R^F = C(CF_3)_3)$. *Chem. Sci.* **9**, 7058–7068 (2018).

35. Krossing, I., Brands, H., Feuerhake, R. & Koenig, S. New reagents to introduce weakly coordinating anions of type $Al(OR^F)_4^-$: Synthesis, structure and characterization of Cs and trityl salts. *J. Fluor. Chem.* **112**, 83–90 (2001).

36. Johnson, K. R. D. & Hayes, P. G. Cyclometalative C–H bond activation in rare earth and actinide metal complexes. *Chem. Soc. Rev.* **42**, 1947–1960 (2013).

37. Corner, S. C. *et al.* Synthesis of heteroleptic yttrium and dysprosium 1,2,4-tris(trimethylsilyl)cyclopentadienyl complexes. *Aust. J. Chem.* **75**, 684–697 (2022).

38. Harvey, M. J., Hanusa, T. P. & Pink, M. Structural characterization of the columnar alkali metal cyclopentadienide $[K\{C_5H_2(SiMe_3)_3\text{-}1,2,4\}]_\infty$. *J. Chem. Soc., Dalt. Trans.* **2**, 1128–1130 (2001).

39. Gabbaï, F. P. *et al.* An Editorial About Elemental Analysis. *Organometallics* **35**, 3255–3256 (2016).

40. Fadeeva, V. P., Tikhova, V. D. & Nikulicheva, O. N. Elemental analysis of organic compounds with the use of automated CHNS analyzers. *J. Anal. Chem.* **63**, 1094–1106 (2008).

41. Marks, T. J. & Kolb, J. R. Covalent Transition Metal, Lanthanide, and Actinide Tetrahydroborate Complexes. *Chem. Rev.* **77**, 263–293 (1977).

42. Sur, S. K. Measurement of magnetic susceptibility and magnetic moment of paramagnetic molecules in solution by high-field fourier transform NMR spectroscopy. *J. Magn. Reson.* **82**, 169–173 (1989).

43. Liddle, S. T., Mills, D. P. & Natrajan, L. S. *The Lanthanides and Actinides*. (World Scientific Publishing Europe Ltd, 2022). doi:10.1142/q0298.

44. Ortu, F. *et al.* Synthesis and structural characterization of lanthanum and cerium substituted cyclopentadienyl borohydride complexes. *J. Organomet. Chem.* **857**, 45–51 (2018).

45. Bonnet, F. *et al.* Organometallic Early Lanthanide Clusters: Syntheses and X-ray Structures of New Monocyclopentadienyl Complexes. *Inorg. Chem.* **43**, 3682–3690 (2004).

46. Reta, D. & Chilton, N. F. Uncertainty estimates for magnetic relaxation times and magnetic relaxation parameters. *Phys. Chem. Chem. Phys.* **21**, 23567–23575 (2019).

47. Blackmore, W. J. A. *et al.* Characterisation of magnetic relaxation on extremely long timescales. *Phys. Chem. Chem. Phys.* **25**, 16735–16744 (2023).

48. Chilton, N. F. & Reta, D. Extraction of "hidden" relaxation times from AC susceptibility data. *Chem. Squared* **4**, 3 (2020).

49. Giansiracusa, M. J. *et al.* A large barrier single-molecule magnet without magnetic memory. *Dalton Trans.* **48**, 10795–10798 (2019).

50. Thomas, J. R., Giansiracusa, M. J., Mole, R. A. & Sulway, S. A. Increasing the Symmetry around Lanthanide Ions: The Effect on Single-Ion Magnet Behavior and Electronic Structure. *Cryst. Growth Des.* **24**, 573–583 (2024).

51. Liu, J. L., Chen, Y. C. & Tong, M. L. Symmetry strategies for high performance lanthanide-based single-molecule magnets. *Chem. Soc. Rev.* **47**, 2431–2453 (2018).

52. Ding, Y. *et al.* A Study of Magnetic Relaxation in Dysprosium(III) Single-Molecule Magnets. *Chem. – A Eur. J.* **26**, 5893–5902 (2020).

53. Parmar, V. S., Mills, D. P. & Winpenny, R. E. P. Mononuclear Dysprosium Alkoxide and Aryloxide Single-Molecule Magnets. *Chem. – A Eur. J.* **27**, 7625–7645 (2021).

54. Xu, W., Luo, Q., Li, Z., Zhai, Y. & Zheng, Y. Bis-Alkoxide Dysprosium(III) Crown Ether Complexes Exhibit Tunable Air Stability and Record Energy Barrier. *Adv. Sci.* **11**, 2308548(1–8) (2024).

55. Demir, S. *et al.* Slow Magnetic Relaxation in a Dysprosium Ammonia Metallocene Complex. *Inorg. Chem.* **56**, 15049–15056 (2017).

56. Collins, R., Heras Ojea, M. J., Mansikkamäki, A., Tang, J. & Layfield, R. A. Carbonyl Back-Bonding Influencing the Rate of Quantum Tunnelling in a Dysprosium Metallocene Single-Molecule Magnet. *Inorg. Chem.* **59**, 642–647 (2020).

57. Pugh, T., Chilton, N. F. & Layfield, R. A. A Low-Symmetry Dysprosium Metallocene Single-Molecule Magnet with a High Anisotropy Barrier. *Angew. Chem. Int. Ed.* **55**, 11082–11085 (2016).

58. Müller, L. O. *et al.* Simple Access to the Non-Oxidizing Lewis Superacid PhF→Al(OR^F) 3 (R^F =$C(CF_3)_3$). *Angew. Chem. Int. Ed.* **47**, 7659–7663 (2008).

Acknowledgements

We thank The University of Manchester for access to the Computational Shared Facility and the European Research Council (StG-851504 and CoG-816268) and the UK EPSRC (EP/P001386/1, EP/S033181/1 and EP/T011289/1) for funding. We acknowledge the EPSRC UK National Electron Paramagnetic Resonance Service for access to the SQUID magnetometer, and the NNUF EPSRC CRR facilities at the University of Manchester, supported by the National Nuclear User Facility, for access to single crystal XRD.

Author contributions

S.C.C. and D.P.M. provided the original concept. S.C.C. synthesised and characterised the complexes. S.C.C. collected and finalised the SCXRD data. S.C.C. collected the PXRD data sets; G.F.S.W solved and refined the PXRD datasets. S.C.C. performed DFT and *ab initio* calculations. S.C.C. and G.K.G. collected the magnetic data. S.C.C., W.J.A.B. and G.K.G. interpreted the magnetic data. N.F.C. supervised the magnetism and computational components. D.P.M. supervised the synthetic component and directed the research. S.C.C., W.J.A.B., G.K.G., N.F.C and D.P.M. wrote the manuscript, with contributions from all authors.

Competing interests

The authors declare no competing interests.